Sustainable Hydraulics in the Era of Global Change – Erpicum et al. (Eds.)
© 2016 Taylor & Francis Group, London, ISBN 978-1-138-02977-4

Waves generated by ship convoy: Comparison of physical and numerical modeling with in-situ measurements

T. Cohen Liechti, G. De Cesare & A.J. Schleiss
Laboratory of Hydraulic Constructions (LCH), Ecole Polytechnique Fédérale de Lausanne (EPFL), Lausanne, Switzerland

R. Amacher
Laboratory of Applied Mechanics and Reliability Analysis (LMAF), Ecole Polytechnique Fédérale de Lausanne (EPFL), Lausanne, Switzerland

M. Pfister
Filière de génie civil, Haute école d'ingénierie et d'architecture (HEIA-FR, HES-SO), Fribourg, Switzerland

ABSTRACT: A part of the domestic waste of the city of Geneva (Switzerland) is transported with ship convoys on the Rhone River to the waste incineration station. These convoys generate waves, which partially endangers the stability of the river banks and the riparian fauna. To reduce the dominant wave peaks, a flap was added at the stern of the barge. The efficiency of that flap was tested in physical and numerical model tests, and then compared to in-situ measurements. This case study focuses on a discussion of the appropriateness of the two models, by describing their accuracy for the present case. It indicates that the physical model reproduces the wave heights almost correctly, but does not re-produce adequately the dominant frequencies. In contrast, the numerical model damps the wave heights significantly, but gives correct dominant frequencies.

1 INTRODUCTION

Since several decades, a part of the domestic waste of the City of Geneva (Switzerland) is transported on the Rhone River from the city center to the waste incineration station outside of the city with ship convoys consisting of a pusher tug and a barge. The pusher tug has a length of 12.1 m, a width of 5.5 m, and a weight of 52 tons; The barge is 43.0 m long, 8.6 m wide, and weighs 120 tons. The transport capacity of a barge is 170 t.

Waves generated by these convoys may damage the riverbanks and affect the riparian fauna (Nanson et al. 1994, Coops et al. 1996, Bishop 2003, De Roo et al. 2012), requiring consequently protection and maintenance measures. As an efficient approach, a reduction of the convoy velocity is frequently discussed, particularly as the convoy passes a nature reserve. The latter is, however, not appropriate for logistic reasons, so that adaptions on the hull are considered by the Industrial Services of Geneva (SIG) as operator. To specify such adaptions, and to quantify their effect, SIG assigned the Laboratory of Hydraulic Constructions (LCH) of Ecole Polytechnique Fédéral de Lausanne (EPFL) to propose related options and to validate them with physical and numerical model tests. The latter indicated that a flap mounted at the barge stern is effective (Fig. 1), as the waves generated between the pusher tug and the barge are critical. Those are significantly reduced by the flap, as the pusher tug and the barge are hydrodynamically linked. The flap is operated by hydraulic cylinders and lowered during journey, but lifted up in the port to facilitate manoeuvers.

Figure 1. Sketch of pusher tug (left) and barge (right), with wave-reducing flap at barge stern.

SIG owns one pusher tug and four barges, of which one was equipped with the recommended flap. In order to verify its efficiency, SIG appointed LCH with in-situ measurements of the waves generated by two types of barges: (1) modified including the flap, and (2) original, not modified barge without flap (Amacher et al. 2015). To complete the investigation, LCH conducted additional numerical simulations of the prototype situation. The present case study allows thus to compare the wave characteristic derived from two classical engineering design tools: physical and numerical modeling. Furthermore, the latter results compared with the in-situ measurements, in order to assess the reliability of the models. Herein, the efficiency of the flap is thus not in the focus, but the comparison of the two modeling tools with the in-situ tests.

Table 1. Overview of the test program and conditions, with PM = physical model, NM = numerical model, US = upstream, and DS = downstream, all dimensions in prototype values.

Test	1	2	3	4
Direction	US	DS	US	DS
Stern flap	No	No	Yes	Yes
V_R [m/s]	0.35 (PM) 0.98 (in-situ, NM)	0.98 (in-situ, NM)	0.35 (PM) 0.98 (in-situ, NM)	0.98 (in-situ, NM)
V_a convoy [m/s]	4.55 (PM) 3.27 (in-situ, NM)	5.29 (in-situ, NM)	4.55 (PM) 3.35 (in-situ, NM)	5.20 (in-situ, NM)
V_r convoy [m/s]	4.90 (PM) 4.31 (in-situ, NM)	4.25 (in-situ, NM)	4.90 (PM) 4.22 (in-situ, NM)	4.33 (in-situ, NM)
D [m]	7.0 (PM) 8.8 (in-situ, NM)	8.7 (in-situ) 8.3 (NM)	7.0 (PM) 8.8 (in-situ, NM)	9.0 (in-situ) 8.8 (NM)
f_a [Hz]	3.4 (PM) 129.3 (in-situ) 8.2 (NM)	82.2 (in-situ) 8.3 (NM)	3.4 (PM) 132.6 (in-situ) 7.1 (NM)	80.9 (in-situ) 8.3 (NM)

2 WAVE MEASUREMENTS

2.1 *General*

Several tests were conducted with the different model types, of which only representative and, as far as possible, similar cases are selected for the herein given comparison, with the conditions as listed in Table 1. As the downstream journey is not critical for wave generation and the barge was empty for all journeys, downstream scenarios were ignored in the physical model tests and are thus missing in the herein presented comparison. The numerical model was set-up according to in-situ conditions (prototype scale), with the boundary conditions of the latter.

The following notation is use in Table 1: V_R = measured Rhone River flow velocity, V_a = absolute convoy velocity with the ground as reference, V_r = relative convoy velocity with Rhone River flow as reference, D = Distance between considered wave gauge (UDS) and convoy axis, and f_a = acquisition frequency.

2.2 *Physical modeling*

Physical model tests were conducted at 1:30 scale, based on the Froude similitude (LCH 2009, Fig. 2). The hull of the pusher tug and the barge were both modeled using polystyrene foam. The ship models were loaded to adjust the gravity center as well as inertia, and painted for smoothening the surface. The pusher tug was connected to the barge by two rods allowing for a movement along the vertical axis. The tests were conducted in a channel, 2.0 m wide and 47 m long, regulating the flow depth with a shutter gate at the channel end. The discharge was supplied by in-house pumps and measured using a Magnetic Inductive Discharge meter. The convoy was fixed on a motor driven

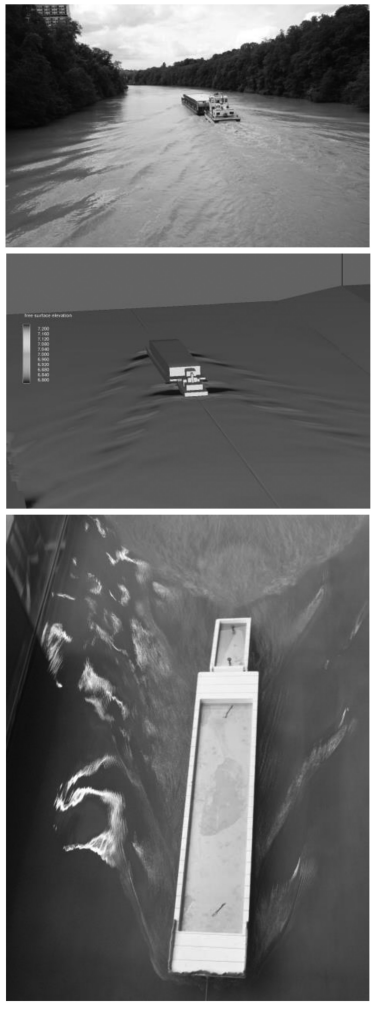

Figure 2. Wave pattern (a) in-situ, as well as in the (b) numerical and (c) physical model.

trolley with velocity control and measurement, which pulled the latter along the channel. The static water levels as well as the wave profiles were locally measured using Ultrasonic Distance Sensors (UDS) installed across the channel at distances D = 7, 12 and 24 m to the streamwise axis of the convoy, again in prototype dimensions. The channel bottom cross-section was rectangular, i.e. not reproducing the effective Rhone River bathymetry. The water depth was fixed at a representative value of 6.0 m, and the discharge was constant 123 m^3/s, both in prototype values.

2.3 *Numerical modeling*

The numerical model was set-up in Flow-3D, version 10 (Flow Science 2011, Fig. 2). Flow-3D numerically solves the continuity and momentum equations using finite-volume approximation. The flow region is subdivided into a mesh of fixed rectangular cells. Within

each cell, local averages of all dependent variables are associated. They are located at the center of the cells except for velocities, which are located at cell faces (staggered grid arrangement). Curved obstacles, wall boundaries, floating objects, or other geometric features are embedded in the mesh by defining the fractional face areas and fractional volumes of the cells that are open to flow (FAVOR method). Most terms in the equations are evaluated using the current time-level values of the local variables explicitly. The two equation k-ε model is used for turbulence closure. The single incompressible fluid with a free surface model was used with no-slip condition on any solid surface boundary, i.e. the river bottom, pusher tug, and barge. The 3D geometry of the pusher tug and barge were inserted as two stereo-lithography (STL) files created in CAD, approximating the surfaces by triangles.

The local bathymetry of the Rhone River was implemented as a sweep of the effective profile with a streamwise regular cross-section width of some 90 m. The pusher tug and the barge were modeled as two individual floating objects, however with similar longitudinal velocities. Their densities were adjusted to achieve a correct immersion, and the gravity center as well as inertia were computed and validated. Near the convoy, a regular meshed grid with cell lengths of 0.100 m vertically, 0.525 m in streamwise direction and 0.500 m transversally was applied, in prototype values. First, the stationary state (water flows in the Rhone River and convoy is immobile at the model end) was simulated during 150 s for each test. Then, a restart was launched with flowing water plus a moving convoy, travelling along a defined path but free to translate in the vertical direction (heave) as well as to rotate around the transverse axis (pitch). The convoy advanced along 100 m in order to generate waves reaching the banks. The waves were derived from sections taken parallel to the path at different distances to the convoy.

2.4 *In-situ measurements*

A reach of the Rhone River with a straight, regular and streamwise constant cross-section of some 90 m width was chosen for the in-situ tests (LCH 2011, Fig. 2). No confluences join the Rhone River along the reach, so that the discharge and the velocities are considered as constant. The Rhone River discharge was 390 m^3/s provided by the Federal Office for the Environment (FOEN) measurement station at Chancy, the flow velocity was measured using ADV (OTT Nautilus C2000), and the maximum flow depth at the talweg was derived as 7.0 m from the bathymetry data. The absolute velocity of the convoy and its path were measured using on-board GPS as well as based on the measurements of the hereafter described LDS. Note that the discharge was smaller in the physical model, being conducted first to define the flap shape.

A 20 m long beam was suspended below the bridge "Passerelle du Lignon", and equipped with four UDS (Baumer UNAM S14) to record the water surface (wave profiles) and a horizontal Laser Distance Sensor (LDS, Micro-Epsilon ILR) to derive the distance between the UDS and the convoy. The effective distance between the UDS and the convoy axis varied at every passage, as a precise path was difficult do drive. The convoy with flap circulated at about 4.5 m distance from the beam, and the convoy without flap at about 2.4 m. As several UDS were mounted along the beam, the UDS closest to the aimed distance of some 9 m was taken into consideration for the comparison with the laboratory tests (Table 1).

3 COMPARISON OF CHARACTERISTIC PARAMETERS

3.1 *Visual observations*

Figure 2 shows the wave pattern as observed in-situ, in the numerical and the physical model. A visual comparison indicates that:

- Three dominant wave packages occur: (1) a first generated at the bow of the barge, (2) a second initiated at the stern of the barge respectively at the bow of the pusher, and (3) a third at the stern of the pusher. The third is, however, close to the second, so they are treated as one package. Note that there is neither an elbow wave for the barge nor for the pusher as they are straight.
- The dominant waves appear basically similar in all pictures.
- The water surface is generally smoother in the models than in-situ, where small waves are visible.

3.2 *Wave profiles*

Wave profiles as measured at distance D according to Table 1 are shown in Fig. 3. The ordinate gives the water level, relative to the static elevation before the passage, and the abscissa gives the time t. The aforementioned dominant wave packages (1) and (2) are recognizable; namely (1) generated by the bow of the barge at $t = 5$ to 10 s including one or two waves, and (2) produced at the stern of the latter and at the bow of the pusher, respectively, at $t = 15$ to 20 s including several waves. The second package contains more waves, being affected by the mentioned flap. If focusing on the wave profiles as indicated by the two models and comparing them with the in-situ measurements, a analogy is evident.

The *physical* model (PM) tends to underestimate the first wave crest at $t = 7$ to 8 s, whereas the wave troughs are correctly represented. Between the first and the second package, waves below the static level occur. As for the second package, the physical model indicates only one single dominant wave. The amplitude of the latter is overestimated. After the second wave package, water levels below the static elevation occur. In general, the physical model shows smooth waves without local irregularities.

The *numerical* model (NM) tends to significantly underestimate the amplitudes at distance D according

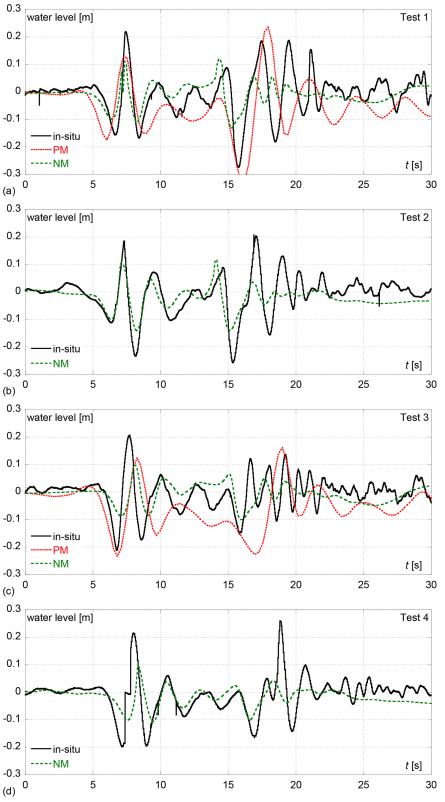

Figure 3. Wave profiles for Tests (a) 1, (b) 2, (c) 3, and (d) 4 (Table 1), from in-situ data, numerical (NM) and physical (PM) model.

to Table 1 due to numeric diffusion. Nevertheless, the first wave package is reconcilable and located at the correct position, but the second is hardly visible. The average water levels between the two wave packages are close to the static elevation. At the end of the measurement reach, the numerical model indicates almost a plain water surface without waves, slightly below the static level. Again, the wave surfaces are smooth and free of local irregularities.

3.3 *Wave heights*

Box plots summarizing the wave profiles over 30 s of acquisition time (similar to Fig. 3) are shown in Fig. 4. Of particular interest are the outliers, which represent the maximum and minimum wave heights. The physical model gives less outliers but with exaggerated values, whereas the numerical model indicates outliers reaching up to some 50% of the maximum in-situ values. The boxes (including 50% of all points) of the physical model are located below the static level, as discussed in the context of Fig. 3, while those of the numerical model are close to it. The box height of the numerical model is slightly smaller than that of the in-situ tests, whereas that of the physical model is significantly bigger.

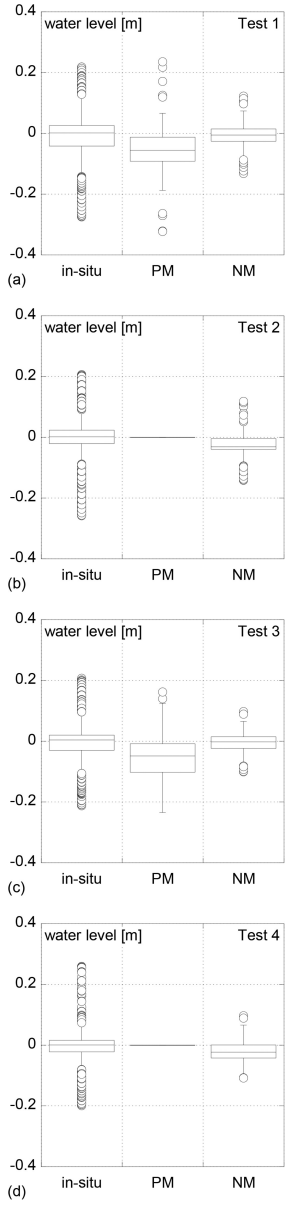

Figure 4. Comparison of wave heights for Tests no (a) 1, (b) 2, (c) 3, and (d) 4 (Table 1).

The wave damping of Test 1 as a function of D is shown in Fig. 5, based on the maximum amplitude of the wave profiles measured over 30 seconds (Fig. 3a). The reduction of the maximum amplitude is similar in-situ and in the physical model, but much smaller for the numerical simulation. Muk-Pavic et al. (2006) report of realistic wave features exclusively close-by a ship hull. The differences are more pronounced if the amplitude closest to the convoy (at minimum value D) is considered as reference, and relating the others to that value. The wave-damping results (Fig. 5b) indicate that the remaining maximum amplitude closest to

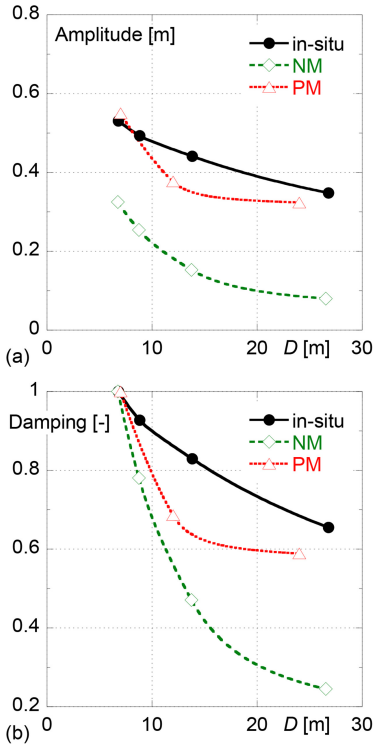

Figure 5. Maximum wave amplitudes as a function of the distance D, (a) in absolute terms, and (b) damping relative to the point measured closest to the convoy.

the river banks is 66% of the reference in-situ, around 59% in the physical model, and only 25% in the numerical model. The transversal damping of the maximum amplitude is thus similarly represented by the physical model, but overestimated by the numerical model.

3.4 *Characteristic wave frequencies*

The power spectral density of the observed waves is estimated based on Welch's averaged modified periodogram method (Welch 1968). The resulting wave frequencies f of the different measurements were thereafter corrected (subscript C) to consider the slightly varying V_r, as the UDS were locally fixed, while the convoy was travelling, so that

$$f_C = f \frac{V_r}{V_r \pm V_R} \tag{1}$$

using "+" for journeys with the flow, and "−" against it. As the minimum (subscript m) wave frequency depends on the relative velocity V_r of the convoy (Newman 1978, Douglas et al. 1985), the power spectra were derived only for higher frequencies than the related f_m given as

$$f_m = \frac{\sqrt{g/2\pi}}{V_r} \cong 0.3 \text{ Hz} \tag{2}$$

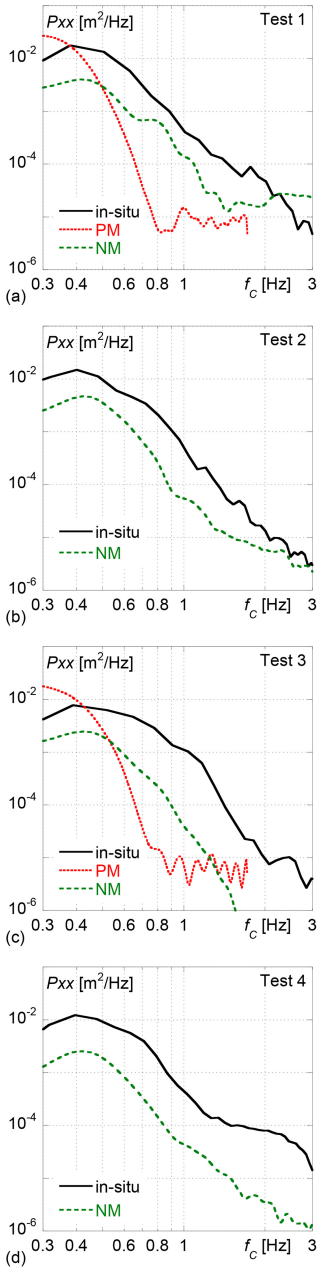

Figure 6. Power spectral densities for Tests no (a) 1, (b) 2, (c) 3, and (d) 4 (Table 1).

Here, g = acceleration due to gravity. Furthermore, the upper frequency limit results from the sampling frequency of the laboratory tests as 1.7 Hz.

In Fig. 6 the power spectral densities *Pxx* of the wave profiles of Fig. 3 are compared. The general trend of the curves is similar; in particular, the numerical model shows a reasonable agreement. The numerical model and the in-situ measurements both indicate a dominant frequency at 0.4 Hz, similar to a typical wave period of 2.5 s representing the two dominant wave

packages. The physical model correctly indicates high energies in low-frequency waves, but gives no explicit value. The high frequencies are underestimated in both models. The physical model gives reliable values up to some 0.8 Hz, whereas exceeding frequencies indicate mainly noise.

4 DISCUSSION

Before discussing some observations, it has to be noted that the conditions of the physical model differed from that of the numerical model and the in-situ tests. The wave profiles of the physical model were recorded at some 80% of the relative distance to the convoy as compared to the numerical model and the in-situ tests, and that the relative convoy velocity was some 15% higher (Table 1). The laboratory flume has a rectangular cross-section and an up-scaled width of 60 m, instead of 90 m in-situ. Finally, the model convoy was pulled while in-situ a propeller feeds the wake zone. The herein presented comparison is thus only indicative.

Regarding a comparison of the wave profiles and therefrom extracted key parameters, the following could be identified regarding the reliability of physical and numerical modeling:

- The physical model correctly reproduces the wave heights, but gives no clear indication on the dominant frequency.
- The numerical model underestimates the wave heights, but correctly reproduces the dominant frequency. Note, however, that the underestimation increases with distance D to the convoy. Waves close to the convoy are represented almost correctly, whereas a numeric diffusion occurs with distance.
- After the first wave package, the physical model indicates too low water levels being significantly below the static reference. This may be a consequence of the relatively narrow channel of the physical model, as compared to in-situ.
- Near the end of the modeled reach, both models indicate water levels slightly below the static reference, ignoring wake waves generated by the propeller. This may be explained with the fact that the UDS are fixed at a location in-situ giving the static level before passage of the convoy, whereas the numerical model gives a section parallel to the convoy course for a fixed time.
- Both models ignore small waves.

5 CONCLUSIONS

It may be assumed that the physical model basically gives accurate results in terms of wave heights, if the boundary conditions are correctly implemented. Information regarding the wave frequency and small waves remain imprecise. The numerical model generates the dominant waves with correct heights near the convoy, but then significantly damps them with distance. Nevertheless, the wave frequencies seem reliable.

Finally, the in-situ tests showed that the flap at the barge stern operates efficiently as mitigation measure, and the two models were able to predict this correctly. The wave heights of the second package, measured near the river banks at $D = 22$ to 24 m were reduced by some 10 to 50%, and the remaining wave energy integrated over 110 s was between 30 to 70%. A generally better agreement would be achieved if the test conditions are identical.

ACKNOWLEDGMENTS

The authors thank the Industrial Services of Geneva (SIG) for the excellent collaboration, in particular Mr. Jan Stefanski.

REFERENCES

Amacher, R., Cohen Liechti, T., Pfister, M., De Cesare, G., Schleiss, A.J. (2015). Wave reducing stern flap on ship convoy to protect riverbanks. *Naval Engineers Journal* 127(1), 95–102.

Bishop, M.J. (2003). Making waves: the effects of boat-wash on macrobenthic assemblage of estuaries. PhD *Thesis*, University of Sydney, A.

Coops, H., Geilen, N., Verheij, H.J., Boeters, R., van der Velde, G. (1996). "Interactions between waves, bank erosion and emergent vegetation: an experimental study in a wave tank." *Aquatic Botany*, 53(3–4), 187–198.

De Roo, S., Vanhaute, L., Troch, P. (2012). "Impact of ship waves on the sediment transport in a nature friendly bank protection." *River Flow* 2012, M. Murillo ed., Taylor & Francis, London.

Douglas, J.F., Gasiorek, J.M., Swaffield, J.A. (1985). *Fluid Mechanics*. Pitman Publishing, London UK.

Flow Science (2011). *Flow-3D User Manual*, Flow Science Inc., Santa Fe, NM, USA

LCH (2009). Transport des déchets ménagers par voie navigable. *Report* 09/2009, Laboratory of Hydraulic Constructions, Ecole Polytechnique Fédérale de Lausanne [unpublished].

LCH (2011). Transport des déchets ménagers par voie navigable sur le Rhône : Efficacité des mesures anti-vagues. *Report* 07/2011, Laboratory of Hydraulic Constructions, Ecole Polytechnique Fédérale de Lausanne [unpublished].

Muk-Pavic, E., Chin, S.N., Spencer, D. (2006). "Validation of the CFD code Flow-3D for the free surface flow around the ships' hulls." 14th *Annual Conference of the* CFD *Society of Canada*.

Nanson, G.C., Krusenstierna, A., Bryant, E.A., Renilson, M.R. (1994). "Experimental measurements on river-bank erosion caused by boat-generated waves on the Gordon River, Tasmania." *Regulated Rivers: Research & Management*, 9(1), 1–14.

Newman, J.N. (1977). *Marine Hydrodynamics*. The MIT Press, Cambridge MA.

Welch, P.D. (1967). "The use of fast Fourier transform for the estimation of power spectra: A meth-od based on time averaging over short, modified periodograms." IEEE Trans. *Audio Electroacoustics*, AU-15, 70–73.